Nano Res (2009) 2: 872–881
DOI 10.1007/s12274-009-9088-6
Research Article

Process Intensification by CO_2 for High Quality Carbon Nanotube Forest Growth: Double-Walled Carbon Nanotube Convexity or Single-Walled Carbon Nanotube Bowls?

Jiaqi Huang, Qiang Zhang, Mengqiang Zhao, and Fei Wei (✉)

Beijing Key Laboratory of Green Chemical Reaction Engineering and Technology, Department of Chemical Engineering, Tsinghua University, Beijing 100084, China

Received: 13 July 2009 / Revised: 2 September 2009 / Accepted: 13 September 2009
©Tsinghua University Press and Springer-Verlag 2009. This article is published with open access at Springerlink.com

ABSTRACT

Introduction of CO_2 is a facile way to tune the growth of vertically aligned double- or single-walled carbon nanotube (CNT) forests on wafers. In the absence of CO_2, a double-walled CNT convexity was obtained. With increasing concentration of CO_2, the morphologies of the forests transformed first into radial blocks, and finally into bowl-shaped forests. Furthermore, the wall number and diameter distribution of the CNTs were also modulated by varying the amount of CO_2. With increasing CO_2 concentration, CNTs with fewer wall number and smaller diameter were obtained. The addition of CO_2 is speculated to generate water and serve as a weak oxidant for high quality CNT growth. It can tune the growth rate and the morphologies of the forests, prevent the formation of amorphous carbon, and reduce the wall number of the CNTs.

KEYWORDS

Carbon nanotube forest, carbon dioxide, chemical vapor deposition, self organization, process intensification

Introduction

Carbon nanotubes (CNTs) have been extensively studied due to their unique mechanical, electronic, and thermal properties [1–3]. CNTs can be considered as a seamless cylinder formed by rolling graphene. The huge aspect ratio helps to generate anisotropic properties along the *c* axis. In vertically aligned form, CNTs have relatively large aspect ratio and good orientation [1, 2], benefiting both the intrinsic performance of CNTs and the facile application of CNT forests [2–6]. The wall number and the diameter of CNTs have been found to affect the properties of CNTs significantly, leading to different applications [5]. Recently, both single- and double-walled CNTs have attracted increasing attention due to their promising applications in field effect transistors, and field emission and electric double-layer capacitors [2, 7–9].

In order to control the wall number distribution of the synthesized CNTs, precisely controlled catalyst layers with different thickness are commonly employed to modulate the size of catalyst particles and the CNTs [5, 10–14]. It is believed that the wall

Address correspondence to wf-dce@tsinghua.edu.cn

number distribution depends strongly on the nominal thickness of the catalyst film. Generally, CNTs with fewer walls grow on thinner catalyst films. Deposition through nano-templates can also control the catalyst size, leading to the preferential growth of wall-number selected CNTs [15]. Delicate control of the annealing process has also been adopted to tune the wall number distribution of as-grown CNTs [16].

These results are important for the development of a standard process for mass production of aligned single-walled CNT forests. Process intensification, which is widely accepted by chemical engineers, should be considered to improve the efficiency and lower the production cost of this process [17]. The process of mass production of CNTs, especially single-walled CNTs (SWCNTs), can be greatly intensified by the introduction of a gaseous oxidizer. For example, in the so-called "super growth" of single-walled CNT forests, the product was strongly affected by the water content in the reactor. Oxygen-containing gases have been tested in the chemical vapor deposition (CVD) process, and they showed great ability to modulate the structure of CNTs [18–21]. It is commonly believed that the addition of water or steam can promote the synthesis of CNT forests, prolong the lifetime of catalyst particles, and prevent the sintering of iron particles [22–25]. Water can also open the end of CNTs by selective etching, which also shows great potential for the delicate tuning of the fine structure of CNTs [26, 27]. Furthermore, it should be noted that CO_2 is also a good weak oxidant which promotes the growth of CNTs [28, 29]. Compared with water, the flow rate of CO_2 can be more easily controlled and it does not condense in the pipeline at room temperature. However, the effect of CO_2 promotion on the growth of CNT forests is not yet fully understood [30, 31].

In this contribution, CO_2 was selected as a promoter to develop a highly efficient process for the synthesis of aligned CNTs with controlled morphology and structure. The morphologies of CNT forests were modulated by controlling the concentration of CO_2 in the CVD growth period. By varying the amount of CO_2, various kinds of forests can be obtained on the same substrate and multi-layered forests can also be fabricated.

1. Experimental

Electron beam evaporation was employed to deposit Al_2O_3 (10.0 nm), Fe (1.0 nm), and MgO (1.0 nm) sequentially on a silicon wafer with SiO_2 of 600 nm thickness as catalyst. The silicon wafer was then cut into small pieces (5.0 mm × 5.0 mm) and put into a quartz tube with an inner diameter of 30 mm and length of 1200 mm for CVD growth. In a typical growth process, the quartz tube containing the substrate was positioned in the tube furnace under the protection of Ar and H_2 and the temperature was raised. When the temperature reached 750 °C, CO_2 and C_2H_4 were introduced into the quartz tube to start the synthesis of CNT forests. The flow rates of Ar, H_2, and C_2H_4 were 250, 200, and 100 standard cubic centimeters per minute (sccm), respectively. The concentration of CO_2 was varied in order to modulate the growth of CNT forests. After a 1-h growth of CNT forests, the supply of C_2H_4 and CO_2 was shut off and the reaction chamber was cooled down under the protection of Ar and H_2.

The morphology of the CNT forests was characterized by a JSM 7401F high-resolution scanning electron microscope (SEM) operated at 5.0 kV and a JEM 2010 high-resolution transmission electron microscope (TEM) operated at 120.0 kV. The sample for the TEM observation was prepared by a common sonication method. Raman experiments were performed with a Renishaw RM2000 Raman spectrophotometer. The spectra were recorded using a He–Ne laser excitation line at 633.0 nm with a spot size of about 20 μm^2 on the CNT forest kept at ambient temperature. To investigate the thermal stability of the CNT forests, thermogravimetry (TG) was carried out on a TGA Q500 instrument, using CO_2 as the atmosphere and with a temperature ramp rate of 10 °C / min.

2. Results and discussion

2.1 Tailoring the morphologies of CNT forests

Figures 1(a)–1(f) show SEM images of the CNT forests grown on a silicon wafer with different CO_2 concentrations. The heights of the CNT forests at

the edges were shorter than those in the center of the substrate (Figs. 1(a), 1(c), and 1(e)). A woven-structured top surface composed of CNTs entangling with each other was formed due to the synchronous growth mode of CNT forests [32]. Vertically aligned convex-shaped, radial-shaped, and bowl-shaped CNT forests can be obtained under different CO_2 concentrations.

A convex-shaped CNT forest was obtained without the addition of CO_2. The height of the middle part of the forest was about 0.4 mm (Fig. 1(a)). A few cracks (three in this case) can be found on the top of the forest (Fig. 1(b)). The width of the cracks was less than 100 μm. The as-grown CNT forest with a CO_2 concentration of 6.5 mol% is shown in Fig. 1(c). The height of the CNT forests in their middle part reached about 1.1 mm. Compared with the growth without CO_2, the nonuniformity of the growth rate was larger and the CNT film split into many blocks. As can be seen from Fig. 1(d), over ten cracks were present on the top surface of the forest, and the width of cracks reached 300 μm. The shape of the as-grown CNT forest was similar to that obtained through radial growth on spherical substrates [33]. Due to the difference in growth rate, every block tended to lean towards the edge of the substrate.

Under high CO_2 concentration (30.4 mol%), forests with an arc-shaped bottom were formed by the sequential fracture of CNTs. The as-grown CNT forest split at the edge of the substrate (Fig. 1(e)) and a uniform height of about 0.55 mm was obtained over the whole as-grown forest. The top view of the forest (Fig. 1(f)) showed a continuous top structure with few cracks. The enlarged image of the top part of the forest (Fig. 1(g)) shows the detailed structure where the split occurred. Part I is composed of continuous vertically aligned CNTs and the lines in the image represent the sides of the assembled CNTs. Part II is composed of the roots of the aligned CNTs, which sequentially rupture at the root from the outermost parts of the whole forest. Due to the continuous growth of the CNT forest and the fracture at the edge of the substrate, CNT roots can be observed from the side of the forest. Figure 1(h) shows the relationship between the forest and the substrate in Fig. 1(e). Some short CNTs are attached to the edge of the substrate, corresponding to the top parts of the CNT forests (Part I in Fig. 1(g)). The rupture of CNT roots from the substrate continued when prolonging the growth duration, and the forest may even detach itself from the substrate over long growth periods under high CO_2 concentrations. Figure 1(i) shows the

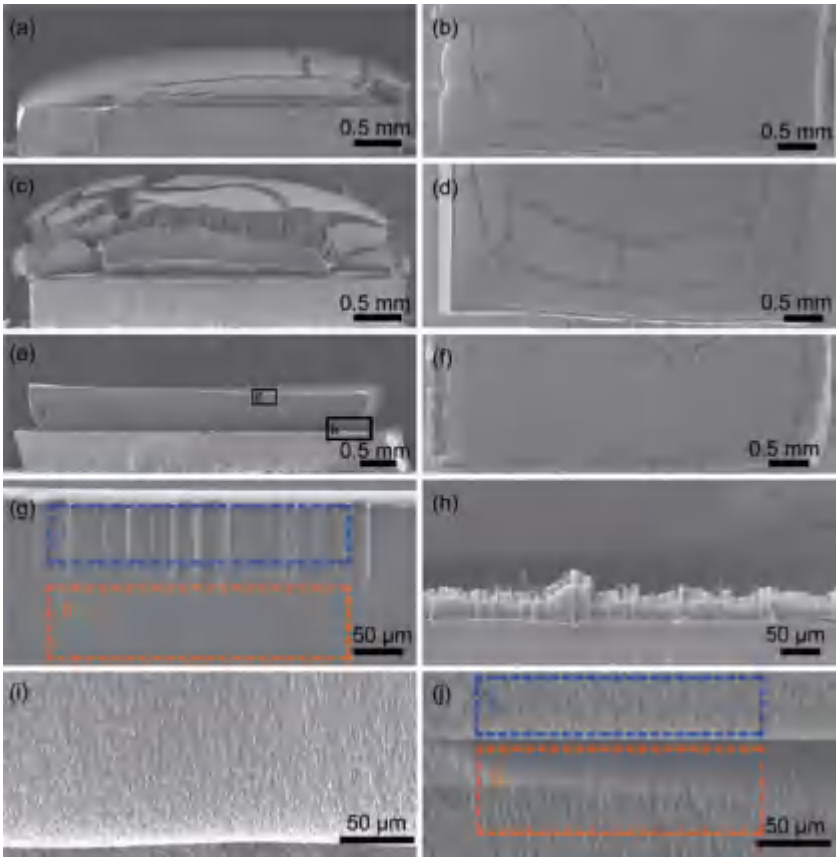

Figure 1 Side view and top view SEM images of CNT forests obtained with CO_2 concentrations of ((a), (b)) 0 mol%, ((c), (d)) 6.5 mol%, and ((e), (f)) 30.4 mol%; (g) enlarged view of the side of CNT forests composed of (I) vertically aligned CNTs and (II) aligned roots of CNTs; (h) enlarged view showing the forest bottom, and the small fraction of CNT forest on the edge and the silicon wafer; (i) the bottom part of the forest composed of aligned CNT roots; (j) the interface of a two-layered CNT forest obtained with 30.4 mol% CO_2: both layers exhibit bowl-liked morphologies with (I) the bottom part of the first layer composed of CNT roots, and (II) the top part of the second layer composed of short vertically aligned CNTs and the aligned CNT roots

bottom of the detached forest, which consists of CNT roots and shows an arc-shaped outer surface. When a two-layered CNT forest was obtained by the carbon source interruption method, the same bowl-liked shape was found in both layers of forests (Fig. 1(j)). Part I is the bottom area of the first layer composed of fractured CNTs. Part II shows the second layer composed of an ordered forest structure and the fractured roots, which is similar to that in Fig. 1(g).

To investigate the generality of this phenomenon, the growth of CNT forests with different CO_2 concentrations was also performed at growth temperatures of 730 °C, 770 °C, and 790 °C and on patterned catalysts. Though the growth behavior differed slightly at different growth temperatures, the same trend of morphology evolution from convex-shaped forests to bowl-liked forests with increasing CO_2 concentration was observed (Figs. S-1–S-3 in the Electronic Supplementary Material (ESM)). The forests grown on the patterned catalyst also exhibited similar behavior in each lattice (Fig. S-4 in the ESM).

Nonuniform growths of CNT forests on the edge and in the middle of substrates have been widely reported [24, 34–37]. The structure of the forests will be discussed in the following section to illustrate the nonuniform self organization of CNTs.

2.2 Modulating the structure of CNTs in the forests

The as-grown CNT forests were further characterized by high-resolution electron microscopy. The top surface structure, cross-section view, and fine structure of CNTs obtained under various CO_2 concentrations are illustrated in Fig. 2. It is commonly believed that during the formation of CNT forests, the CNTs firstly construct a woven structure by entangling with each other. With continuous growth of the CNTs, a vertically aligned CNTs forest structure can subsequently be self-assembled *via* synchronous growth [32]. From the left column in Fig. 2, it can be seen that an entangled CNT woven structure was formed, and the aligned CNTs are shown in the middle column of Fig. 2. Without the addition of CO_2, the woven structure in the top of the forest was covered by a large quantity of carbon impurities such that single CNTs can hardly be distinguished in the SEM images (Fig. 2(a)). The carbonaceous impurities accumulated on CNT forests, especially on the top surface of forests, have been attributed to the pyrolysis of ethylene in the gas phase and deposition on the surface of the CNTs, and the accumulation becomes severe with prolonged CVD duration [38–40]. Figure 2(d) shows the surface obtained with a

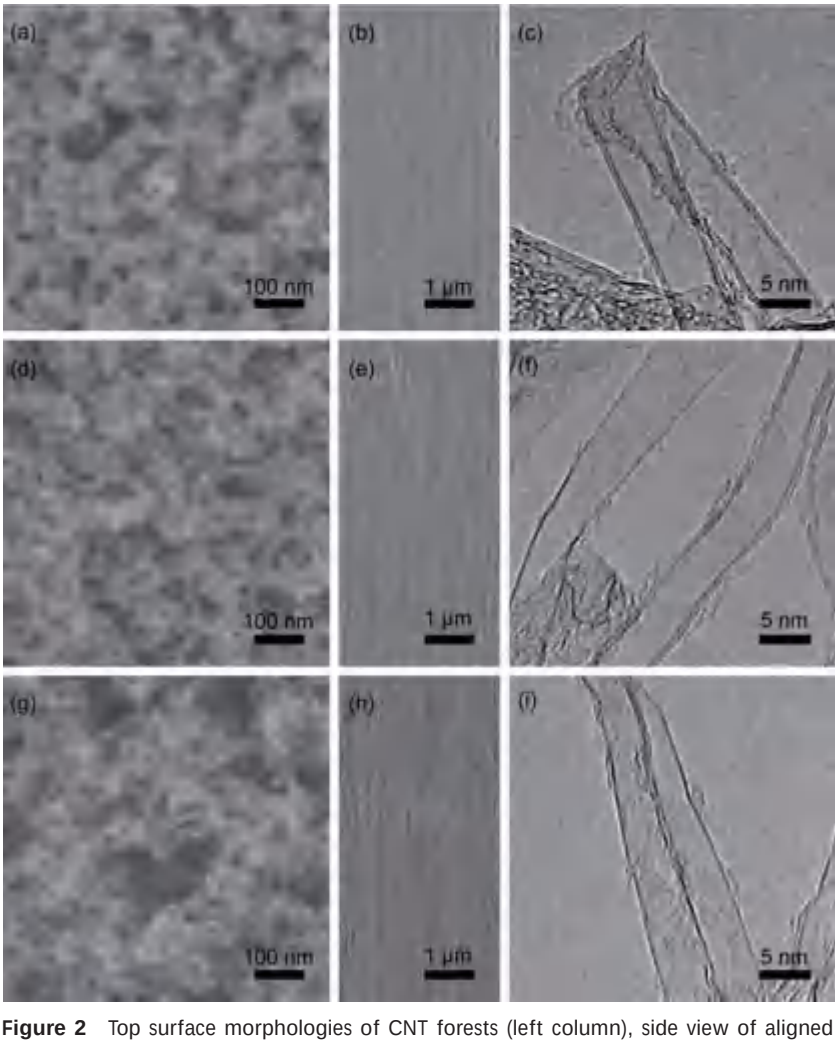

Figure 2 Top surface morphologies of CNT forests (left column), side view of aligned CNT forests (middle column), and high-resolution TEM images of constituent CNTs (right column) of CNT forests obtained with CO_2 concentrations of 0 mol% (top row), 12.5 mol% (middle row), and 30.4 mol% (bottom row)

low CO_2 concentration (12.5 mol%). The top woven structure was appreciably cleaner than that obtained without CO_2 addition, although there were still some carbonaceous impurities coating the CNTs. When further increasing the concentration of CO_2 (to 30.4 mol%), amorphous carbon was mostly eliminated, leaving clean and bare CNTs on the top surface of the CNT forests (Fig. 2(g)). Meanwhile, these CNTs were found to be sparser and less entangled compared with the CNT forests obtained with lower or no CO_2 addition.

As described above, the amount of carbonaceous impurities varied with the concentration of CO_2 in the CVD process. Raman spectroscopy was employed to identify the carbonaceous impurities. Spots were taken in the middle of the side of the CNT forests obtained with various CO_2 concentrations (Fig. 3(a)). In a typical Raman spectrum, the G band (near 1580 cm^{-1}) and the D band (near 1340 cm^{-1}) represent the resonance peak of graphite and the scattering peak of the disordered component, respectively. Therefore, the intensity ratio (I_G/I_D) is commonly used to characterize the crystallization degree of CNT samples. The variation in I_G/I_D with CO_2 concentration is shown in Fig. 3(b). The I_G/I_D was maintained at about 1.0 until the CO_2 concentration was over 15 mol%, after which the I_G/I_D increased dramatically and almost linearly. The I_G/I_D for the CNT forest obtained with a CO_2 concentration of 36.8 mol% reached 2.37, indicating a relatively low content of carbonaceous impurities. This plot confirms that the CO_2 did not significantly oxidize the sample at low CO_2 concentrations and appreciable oxidation only occurred when the concentration was over 15 mol%, after which the oxidation effect increased with the increasing CO_2 concentration. To compare the stability of CNT forests obtained under different CO_2 concentrations, TG analysis under a CO_2 atmosphere was employed. The temperature of the mass loss peak appeared to increase with increasing CO_2 concentration during the synthesis process, indicating the enhanced stability of CNTs synthesized in the presence of CO_2 arising from the selective oxidation (Fig. 3(c)).

The high-resolution TEM images (right column in Fig. 2) show the fine structure of the as-grown CNTs in the forest under different conditions, and reveal the differences in the diameter and the wall number. Briefly, the forest obtained without CO_2 mainly consisted of double-walled CNTs (DWCNTs) (Fig. 2(c)) while single-walled CNTs are in the majority when higher CO_2 concentrations were employed (Fig. 2(i)). The wall number and diameter distributions of CNTs in forests obtained under different conditions were calculated based on the

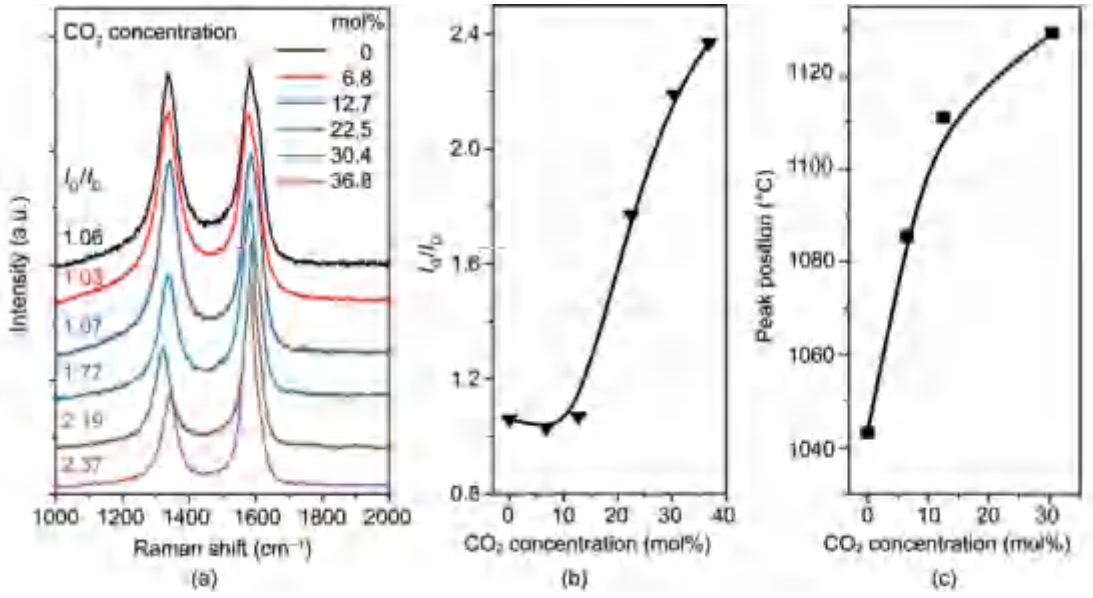

Figure 3 (a) Raman spectra of CNT forests obtained with addition of different amounts of CO_2, (b) plot of the I_G/I_D ratio of the CNT forests, and (c) the peak positions of the mass loss (TG under CO_2 atmosphere) for CNT forests obtained with different CO_2 concentrations

statistics for over two hundred CNTs. Figure 4(a) illustrates the wall number distribution of the as-grown CNTs. As indicated by the stack bars, without CO_2 addition the content of double-walled CNTs was near 50% and the content of single-walled CNTs was below 20%. For CNTs grown with the assistance of CO_2, the content of single-walled CNTs increased gradually with increasing concentration of CO_2. The content of single-walled CNTs was near 40% when the CO_2 concentration was 12.7 mol% and 22.5 mol%. When the CO_2 concentration was further increased to 30.4 mol% and 36.8 mol%, the content of single-walled CNTs reached 63% and 71%, respectively. Together with the increase in content of single-walled CNTs, formation of CNTs with large wall numbers (triple- and multi-walled) was not observed at high levels of CO_2. Besides its role in modulating the wall number distribution, the presence of CO_2 in the growth atmosphere can also change the diameter of CNTs. As indicated by Fig. 4(b), the mean diameters of CNTs in the forest were negatively correlated with the concentration of CO_2. By introducing CO_2 with a concentration of 36.8 mol%, the average outer diameter decreased from 4.30 nm to 3.83 nm. The mean diameters of the inner shell of CNTs were around 3.8 nm and did not differ significantly with changing CO_2 concentration, indicating that the addition of CO_2 did not obviously alter the size of the iron particles.

Since the fine structure of CNTs in the forest can be modulated by the concentration of CO_2 introduced, a two-stage growth of CNTs was conducted to further demonstrate the effect of CO_2 on the growth of CNTs. The two CO_2 concentrations were 30.4 mol% and 6.5 mol%, and the duration of each stage was 30 min. According to the SEM image shown in Fig. 5(a), the forest can be divided into two layers and there was an obvious interface at the middle section of the forest. The heights of the two layers were 380 μm and 320 μm, respectively. The forest possessed a similar bowl-liked shape to those obtained in the presence of CO_2 described above. The first layer (Part I) of the forest was grown under higher CO_2 concentration, leading to a relatively high content of single-walled CNTs, as indicated by the high-resolution TEM image and the pie chart (Figs. 5(b) and 5(c)). The content of the single-walled CNTs was 65.3% while the content of double-walled CNTs was 29.5% and CNTs with large wall number were almost entirely absent. Due to the relatively low concentration of CO_2 during the growth of the bottom (Part II) of the forest, the CNTs in this part were composed of more graphite layers. The contents of single-walled CNTs and double-walled CNTs were 50.5% and 38.3%, respectively, leaving over 10% of triple- or multi-walled CNTs in the forest.

2.3 Mechanism of the tuning effect induced by CO_2

As shown in the above section, both the forest morphologies and CNT structures were modulated

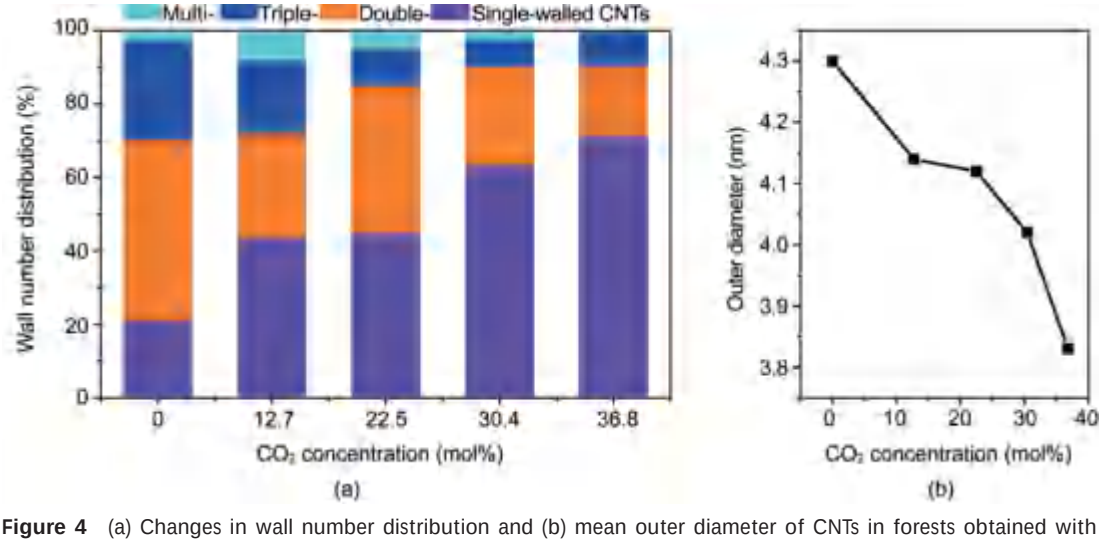

Figure 4 (a) Changes in wall number distribution and (b) mean outer diameter of CNTs in forests obtained with different CO_2 concentrations

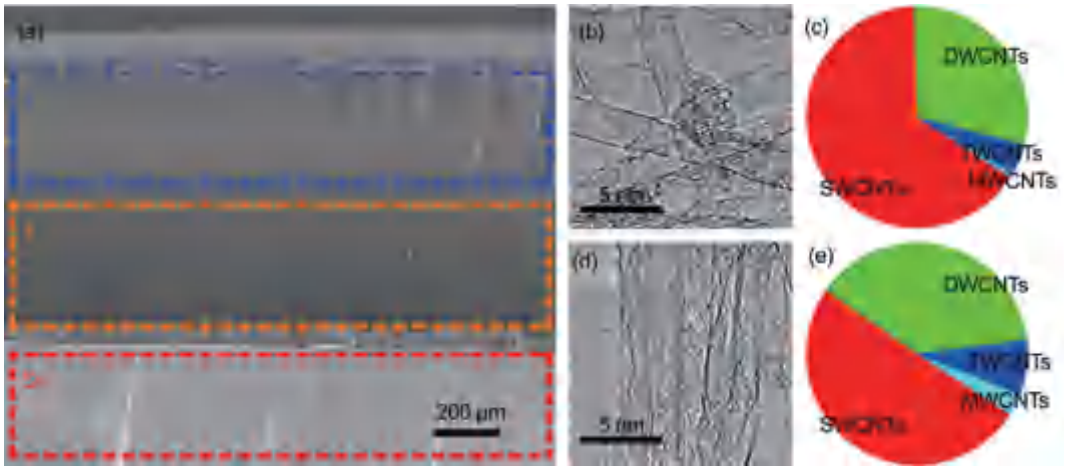

Figure 5 (a) SEM image of two-layered CNT forest, with I indicating the first layer and II representing the second layer; high-resolution TEM images of constituent CNTs of (b) I and (d) II; pie charts of the wall number distribution of CNTs in (c) I and (e) II

by CO_2 addition. In the CVD process, the introduced CO_2 can react with H_2 and generate H_2O, which may boost the growth of CNT forests. Excess CO_2 also acts as a weak oxidant which reacts with the deposited solid carbon, resulting in the observed changes in the forest morphologies and the structure of the CNTs (Fig. 6).

The changes in the morphologies of the CNT forests can be mainly attributed to the changes in the growth rate of the CNT forests and the modulation of the CNT-substrate adhesive force. Millions of CNTs synchronously grow into a forest [32]. In our case, the density of CNTs in the array was estimated to be 2300–2600 μm^{-2}, which is lower than "super growth" (5200 μm^{-2}) [24], alcohol assisted growth (8500 μm^{-2}) [41], or plasma enhanced growth (14000 μm^{-2}) [14]. The sparse density of CNTs suggests that the ability to form the initial top woven structure is a key factor. In the middle section of the substrate, CNTs can easily form the woven structure and grow into a high forest [32], while at the edge, the difficulty in forming the woven structure limits the growth rate, and a CNT convexity is formed. The nonuniformity in growth rate also induces internal stress distributed throughout the CNT forests [32, 37]. With the growth of CNT forests, the stress accumulates. Due to the strong bonding between CNT forests and the substrate, the forests invariably split on the top surface to release the internal stress. Without CO_2 addition, only a few cracks form due to the difference in growth rates on the edge and in the middle of the substrate, and the whole forest possesses a convex shape. With the addition of 6.5 mol% CO_2, the growth of CNT forests in the middle part is dramatically boosted (from 0.4 mm/h without CO_2 to 1.1 mm/h under 6.5 mol% CO_2), which enlarges the nonuniformity in growth rate. Accordingly, the CNT forests split into a large number of blocks and many cracks form.

For high CO_2 concentrations, the bowl-liked forests were formed due to the reduced CNT-substrate adhesive force. Generally, CNTs bond firmly to the substrate with the catalyst between them. The

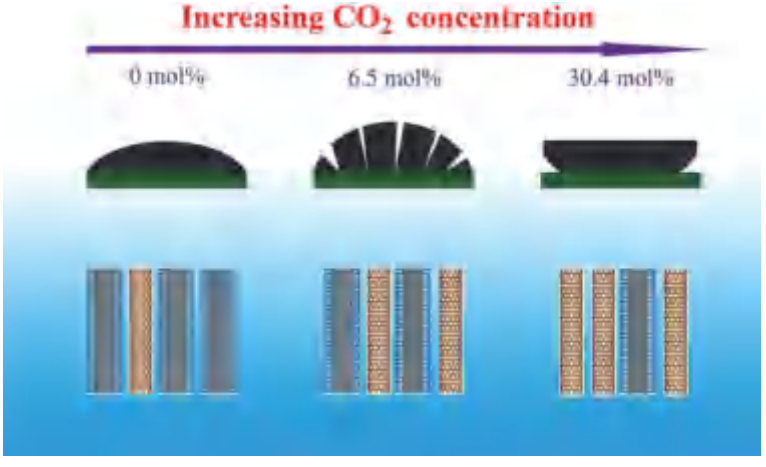

Figure 6 Schematic diagram of the evolution of the forest morphology (middle panel) and the approximate resulting wall number distribution of CNTs in the forest (bottom panel) with increasing CO_2 concentration

presence of certain substance can etch the catalyst or the deposited carbon near the catalyst and reduce the CNT-substrate adhesive force [42]. The CNTs near the iron particles were preferentially etched due to the catalytic oxidation by high concentrations of CO_2. At the initial stage of CNT growth, the forest split on the edge because of the weak bonding between CNT forests and the substrate, leaving some residual forest on the edge of substrate. With the further growth of the forest, the outermost part of the forest continuously detached from the substrate, resulting in the bowl-shaped morphology. It is worth mentioning that the stress in the forests was released by the rupture of forests from the substrates and the nonuniformities of growth rate were eliminated, leaving a complete top surface structure of the forests.

The CO_2 also changes the structure of CNTs in the forest through oxidative etching. Small amounts of CO_2 reacted with H_2 and the oxidative etching of solid carbon was not obvious. However, higher concentrations of CO_2 can cause the oxidation of both as-grown CNTs and carbonaceous impurities. Generally, the amorphous carbon and the incomplete graphite layers react more readily with CO_2 compared with the well-graphitized CNT walls. Thus, the amorphous carbon contained in the CNT forests could be completely eliminated by increasing CO_2 addition and the I_G/I_D increased accordingly (Fig. 3(b)). Accompanying the etching of amorphous carbon, the complete graphite layers of CNTs (especially the outer walls of CNTs) were inevitably slightly etched by CO_2. As a result, this process can tune the wall number distribution of the CNTs in the forests. The wall number of the CNTs decreased gradually with increasing CO_2 concentration.

Finally, it should be noted that by CO_2 addition, the morphology and CNT selectivity in the as-grown forest can be modulated easily. With the increase of CO_2 concentration from 0 mol% to 36.8 mol%, the content of single-walled CNTs increased from 20% to over 70%. Even for CNT forests radially grown on spheres [33], flying carpets on flakes [43], forests intercalated in lamellar clays [44] and the odako growth of dense CNT forests [45], CO_2 addition can be expected to play an important role in easily modulating the growth behavior both in a fixed bed or a fluidized bed reactor.

3. Conclusions

Introduction of CO_2 into the CVD process allows controllable synthesis of single- or double-walled CNT forests. Both the CNT forest morphology and CNT structure were modulated by the introduction of CO_2. When the CO_2 concentration was increased from 0 mol% to 30.4 mol%, the morphology of CNT forests changed from convex-shaped to radial-block-shaped and then to bowl-shaped. By introducing large amounts of CO_2, the carbonaceous impurities can be eliminated and the wall number of CNTs can also be significantly reduced. When the CVD atmosphere comprised 36.8 mol% of CO_2, the content of single-walled CNTs in the forest reached 70%. It is suggested that the addition of CO_2 generates water and serves as a weak oxidant to modulate both the morphology of the forest and the structure of the CNTs. CO_2-assisted growth is therefore a facile way for the controllable synthesis of CNT forests, and also provides a further general understanding of process intensification for nanostructure modulation.

Acknowledgements

The work was supported by the National Natural Science Foundation of China (Nos. 20736007 and 2007AA03Z346), and the China National Basic Research Program (No. 2006CB0N0702).

Electronic Supplementary Material: SEM images of CNT forests grown with varying concentrations of CO_2 at different temperatures on a silica substrate as well as on a patterned catalyst are available in the online version of this article at http://dx.doi.org/10.1007/s12274-009-9088-6 and are accessible free of charge.

References

[1] Li, W. Z.; Xie, S. S.; Qian, L. X.; Chang, B. H.; Zou, B. S.; Zhou, W. Y.; Zhao, R. A.; Wang, G. Large-scale synthesis of aligned carbon nanotubes. *Science* **1996**, *274*, 1701–

1703.

[2] Fan, S. S.; Chapline, M. G.; Franklin, N. R.; Tombler, T. W.; Cassell, A. M.; Dai, H. J. Self-oriented regular arrays of carbon nanotubes and their field emission properties. *Science* **1999**, *283*, 512–514.

[3] Dai, L. M.; Patil, A.; Gong, X. Y.; Guo, Z. X.; Liu, L. Q.; Liu, Y.; Zhu, D. B. Aligned nanotubes. *ChemPhysChem* **2003**, *4*, 1150–1169.

[4] Qu, L. T.; Dai, L. M.; Stone, M.; Xia, Z. H.; Wang, Z. L. Carbon nanotube arrays with strong shear binding-on and easy normal lifting-off. *Science* **2008**, *322*, 238–242.

[5] Liu, K.; Sun, Y. H.; Chen, L.; Feng, C.; Feng, X. F.; Jiang, K. L.; Zhao, Y. G.; Fan, S. S. Controlled growth of super-aligned carbon nanotube arrays for spinning continuous unidirectional sheets with tunable physical properties. *Nano Lett.* **2008**, *8*, 700–705.

[6] Zhang, Q.; Xu, G. H.; Huang, J. Q.; Zhou, W. P.; Zhao, M. Q.; Wang, Y.; Qian, W. Z.; Wei, F. Fluffy carbon nanotubes produced by shearing vertically aligned carbon nanotube arrays. *Carbon* **2009**, *47*, 538–541.

[7] Dai, H. J.; Javey, A.; Pop, E.; Mann, D.; Kim, W.; Lu, Y. R. Electrical transport properties and field effect transistors of carbon nanotubes. *Nano* **2006**, *1*, 1–13.

[8] Frackowiak, E.; Beguin, F. Carbon materials for the electrochemical storage of energy in capacitors. *Carbon* **2001**, *39*, 937–950.

[9] Zhong, G. F.; Iwasaki, T.; Robertson, J.; Kawarada, H. Growth kinetics of 0.5 cm vertically aligned single-walled carbon nanotubes. *J. Phys. Chem. B* **2007**, *111*, 1907–1910.

[10] Chakrabarti, S.; Kume, H.; Pan, L. J.; Nagasaka, T.; Nakayama, Y. Number of walls controlled synthesis of millimeter-long vertically aligned brushlike carbon nanotubes. *J. Phys. Chem. C* **2007**, *111*, 1929–1934.

[11] Patole, S. P.; Alegaonkar, P. S.; Shin, H. C.; Yoo, J. B. Alignment and wall control of ultra long carbon nanotubes in water assisted chemical vapour deposition. *J. Phys. D: Appl. Phys.* **2008**, *41*, 155311.

[12] Xiong, G. Y.; Wang, D. Z.; Ren, Z. F. Aligned millimeter-long carbon nanotube arrays grown on single crystal magnesia. *Carbon* **2006**, *44*, 969–973.

[13] Zhao, B.; Futaba, D. N.; Yasuda, S.; Akoshima, M.; Yamada, T.; Hata, K. Exploring advantages of diverse carbon nanotube forests with tailored structures synthesized by supergrowth from engineered catalysts. *ACS Nano* **2009**, *3*, 108–114.

[14] Zhong, G. F.; Iwasaki, T.; Kawarada, H. Semi-quantitative study on the fabrication of densely packed and vertically aligned single-walled carbon nanotubes. *Carbon* **2006**, *44*, 2009–2014.

[15] Lee, D. H.; Lee, W. J.; Kim, S. O. Highly efficient vertical growth of wall-number-selected, N-doped carbon nanotube arrays. *Nano Lett.* **2009**, *9*, 1427–1432.

[16] Iwasaki, T.; Maki, T.; Yokoyama, D.; Kumagai, H.; Hashimoto, Y.; Asari, T.; Kawarada, H. Highly selective growth of vertically aligned double-walled carbon nanotubes by a controlled heating method and their electric double-layer capacitor properties. *Phys. Stat. Sol. (RRL)* **2008**, *2*, 53–55.

[17] Wei, F.; Zhang, Q.; Qian, W. Z.; Yu, H.; Wang, Y.; Luo, G. H.; Xu, G. H.; Wang, D. Z. The mass production of carbon nanotubes using a nano-agglomerate fluidized bed reactor: A multiscale space-time analysis. *Powder Technol.* **2008**, *183*, 10–20.

[18] Wu, Z. P.; Wang, J. N.; Ma, J. Methanol-mediated growth of carbon nanotubes. *Carbon* **2009**, *47*, 324–327.

[19] Zhang, G. Y.; Mann, D.; Zhang, L.; Javey, A.; Li, Y. M.; Yenilmez, E.; Wang, Q.; McVittie, J. P.; Nishi, Y.; Gibbons, J. ; Dai, H. J. Ultra-high-yield growth of vertical single-walled carbon nanotubes: Hidden roles of hydrogen and oxygen. *P. Natl. Acad. Sci. USA* **2005**, *102*, 16141–16145.

[20] Murakami, Y.; Chiashi, S.; Miyauchi, Y.; Hu, M. H.; Ogura, M.; Okubo, T.; Maruyama, S. Growth of vertically aligned single-walled carbon nanotube films on quartz substrates and their optical anisotropy. *Chem. Phys. Lett.* **2004**, *385*, 298–303.

[21] Sugime, H.; Noda, S.; Maruyama, S.; Yamaguchi, Y. Multiple "optimum" conditions for Co–Mo catalyzed growth of vertically aligned single-walled carbon nanotube forests. *Carbon* **2009**, *47*, 234–241.

[22] Amama, P. B.; Pint, C. L.; McJilton, L.; Kim, S. M.; Stach, E. A.; Murray, P. T.; Hauge, R. H.; Maruyama, B. Role of water in super growth of single-walled carbon nanotube carpets. *Nano Lett.* **2009**, *9*, 44–49.

[23] Yamada, T.; Maigne, A.; Yudasaka, M.; Mizuno, K.; Futaba, D. N.; Yumura, M.; Iijima, S.; Hata, K. Revealing the secret of water-assisted carbon nanotube synthesis by microscopic observation of the interaction of water on the catalysts. *Nano Lett.* **2008**, *8*, 4288–4292.

[24] Hata, K.; Futaba, D. N.; Mizuno, K.; Namai, T.; Yumura, M.; Iijima, S. Water-assisted highly efficient synthesis of

impurity-free single-walled carbon nanotubes. *Science* **2004**, *306*, 1362–1364.

[25] Liu, J. X.; Ren, Z.; Duan, L. Y.; Xie, Y. C. Effects of H_2O on preparation of single-wall carbon nanotubes (SWCNTs) by catalytic decomposition of CH_4 in Ar. *Acta Chim. Sinica* **2004**, *62*, 775–782.

[26] Zhu, L. B.; Sun, Y. Y.; Hess, D. W.; Wong, C. P. Well-aligned open-ended carbon nanotube architectures: An approach for device assembly. *Nano Lett.* **2006**, *6*, 243–247.

[27] Zhu, L. B.; Xiu, Y. H.; Hess, D. W.; Wong, C. P. Aligned carbon nanotube stacks by water-assisted selective etching. *Nano Lett.* **2005**, *5*, 2641–2645.

[28] Wen, Q.; Qian, W. Z.; Wei, F.; Liu, Y.; Ning, G. Q.; Zhang, Q. CO_2-assisted SWNT growth on porous catalysts. *Chem. Mater.* **2007**, *19*, 1226–1230.

[29] Li, Z. R.; Xu, Y.; Ma, X. D.; Dervishi, E.; Saini, V.; Biris, A. R.; Lupu, D.; Biris, A. S. CO_2 enhanced carbon nanotube synthesis from pyrolysis of hydrocarbons. *Chem. Commun.* **2008**, 3260–3262.

[30] Wu, J.; Ma, Y. F.; Tang, D. M.; Liu, C.; Huang, Q. W.; Huang, Y.; Cheng, H. M.; Chen, D. P.; Chen, Y. S. Enhancement of field emission of CNTs array by CO_2-assisted chemical vapor deposition. *J. Nanosci. Nanotechnol.* **2009**, *9*, 3046–3051.

[31] Pint, C. L.; Pheasant, S. T.; Parra-Vasquez, A. N. G.; Horton, C.; Xu, Y. Q.; Hauge, R. H. Investigation of optimal parameters for oxide-assisted growth of vertically aligned single-walled carbon nanotubes. *J. Phys. Chem. C* **2009**, *113*, 4125–4133.

[32] Zhang, Q.; Zhou, W. P.; Qian, W. Z.; Xiang, R.; Huang, J. Q.; Wang, D. Z.; Wei, F. Synchronous growth of vertically aligned carbon nanotubes with pristine stress in the heterogeneous catalysis process. *J. Phys. Chem. C* **2007**, *111*, 14638–14643.

[33] Zhang, Q.; Huang, J. Q.; Zhao, M. Q.; Qian, W. Z.; Wang, Y.; Wei, F. Radial growth of vertically aligned carbon nanotube arrays from ethylene on ceramic spheres. *Carbon* **2008**, *46*, 1152–1158.

[34] Yamada, T.; Namai, T.; Hata, K.; Futaba, D. N.; Mizuno, K.; Fan, J.; Yudasaka, M.; Yumura, M.; Iijima, S. Size-selective growth of double-walled carbon nanotube forests from engineered iron catalysts. *Nat. Nanotechnol.* **2006**, *1*, 131–136.

[35] Hart, A. J.; van Laake, L.; Slocum, A. H. Desktop growth of carbon-nanotube monoliths with *in situ* optical imaging. *Small* **2007**, *3*, 772–777.

[36] Nessim, G. D.; Hart, A. J.; Kim, J. S.; Acquaviva, D.; Oh, J. H.; Morgan, C. D.; Seita, M.; Leib, J. S.; Thompson, C. V. Tuning of vertically-aligned carbon nanotube diameter and areal density through catalyst pre-treatment. *Nano Lett.* **2008**, *8*, 3587–3593.

[37] Meshot, E. R.; Hart, A. J. Abrupt self-termination of vertically aligned carbon nanotube growth. *Appl. Phys. Lett.* **2008**, *92*, 113107.

[38] Li, X. S.; Ci, L.; Kar, S.; Soldano, C.; Kilpatrick, S. J.; Ajayan, P. M. Densified aligned carbon nanotube films *via* vapor phase infiltration of carbon. *Carbon* **2007**, *45*, 847–851.

[39] Feng, X. F.; Liu, K.; Xie, X.; Zhou, R. F.; Zhang, L. N.; Li, Q. Q.; Fan, S. S.; Jiang, K. L. Thermal analysis study of the growth kinetics of carbon nanotubes and epitaxial graphene layers on them. *J. Phys. Chem. C* **2009**, *113*, 9623–9631.

[40] Yasuda, S.; Hiraoka, T.; Futaba, D. N.; Yamada, T.; Yumura, M.; Hata, K. Existence and kinetics of graphitic carbonaceous impurities in carbon nanotube forests to assess the absolute purity. *Nano Lett.* **2009**, *9*, 769–773.

[41] Xiang, R.; Yang, Z.; Zhang, Q.; Luo, G. H.; Qian, W. Z.; Wei, F.; Kadowaki, M.; Einarsson, E.; Maruyama, S. Growth deceleration of vertically aligned carbon nanotube arrays: Catalyst deactivation or feedstock diffusion controlled? *J. Phys. Chem. C* **2008**, *112*, 4892–4896.

[42] Pint, C. L.; Xu, Y. Q.; Pasquali, M.; Hauge, R. H. Formation of highly dense aligned ribbons and transparent films of single-walled carbon nanotubes directly from carpets. *ACS Nano* **2008**, *2*, 1871–1878.

[43] Pint, C. L.; Pheasant, S. T.; Pasquali, M.; Coulter, K. E.; Schmidt, H. K.; Hauge, R. H. Synthesis of high aspect-ratio carbon nanotube "flying carpets" from nanostructured flake substrates. *Nano Lett.* **2008**, *8*, 1879–1883.

[44] Zhang, Q.; Zhao, M. Q.; Liu, Y.; Cao, A. Y.; Qian, W. Z.; Lu, Y. F.; Wei, F. Energy-absorbing hybrid composites based on alternate carbon nanotube and inorganic layers. *Adv. Mater.* **2009**, *21*, 2876–2880.

[45] Pint, C. L.; Alvarez, N. T.; Hauge, R. H. Odako growth of dense arrays of single-walled carbon nanotubes attached to carbon surfaces. *Nano Res.* **2009**, *2*, 526–534.